Smart Agricultural Technology 8 (2024) 100464

Contents lists available at ScienceDirect

Smart Agricultural Technology

journal homepage: www.journals.elsevier.com/smart-agricultural-technology

Identification of unique electromagnetic signatures from GLRaV-3 infected grapevine leaves in different stages of virus development.

Leeko Lee [a,*], Andrew Reynolds [b], Yibin Lan [c], Baozhong Meng [d]

[a] Bluebottle Butterfly Inc. 31 Cameron Court, Fredericton E3B 2R9, NB, Canada
[b] Adjunct Professor, University of Guelph and University of Waterloo; 613 Memorial Drive, Fenwick L0S 1C0, ON, Canada
[c] Center for Viticulture and Enology, China Agricultural University, Beijing 100083, China
[d] Dept. of Cell and Molecular Biology, University of Guelph. 50 Stone Rd E, Guelph N1G 2W1, ON, China

ARTICLE INFO

Key words:
Crop stress sensing
Early virus detection
Polymerase chain reaction (PCR)
Grapevine leafroll associated virus 3 (GLRaV-3)
Portable spectrometer
Hyperspectral sensor
Multispectral sensor
Remotely piloted aircraft system (RPAS)

ABSTRACT

Grapevine leafroll associated virus 3 (GLRaV-3) is one of the most common viruses that adversely affect grape production quality around the world. Grapevine virus is usually detected by polymerase chain reaction (PCR) tests, but the main diagnostic challenges with the PCR are uneven distribution of symptoms, low virus titers in early stage, and the tests are time consuming and expensive. In the absence of effective control and treatment for grapevine virus, the recommendation is to remove infected vines before they become a source of transmission and a rapid and early detection method for viruses is urgently needed. This study investigated how GLRaV-3 infection affects spectral behavior of grapevine leaves and the use of remote sensing tools to identify changes caused by the biotic stress. A Real-Time RT-qPCR test was performed to select representative vines with healthy and GLRaV-3 infection, and changes in electromagnetic (EM) spectrum of leaves were observed with a portable hyperspectral spectrometer and a multispectral sensor on a remotely piloted aircraft system (RPAS). The results of this study suggest that foliar EM reflectance may differ depending on the presence or absence of visible symptoms of infected leaves and different stages of virus infection progress could be indicated by changes in the relative rate of reflectance around 700 nm. This research also confirmed that the development of a narrow-band hyperspectral index for the detection of grapevine virus is feasible, further research is recommended in a much more comprehensive investigation including a combination of hyperspectral sensor and chlorophyll fluorescence sensors, interpolation of suspect wavebands into ratios or indices, larger sample sizes and a more controlled study environment.

Introduction

Many vineyards around the world suffer economic losses due to virus infections. Grapevine leafroll associated virus 3 (GLRaV-3) is one such virus that commonly affects grape production quality in nearly every major grape-growing region [1–5]. In most cases, grapevine virus is detected in infected leaf tissue of a vine by amplifying the viral genome sequence with the polymerase chain reaction (PCR) [6]. The main diagnostic challenges with the PCR method are that infected vines have uneven symptom distribution so not all leaves may contain the virus at the same level, new infections are low in virus titer, and multiple viruses can infect grapevines at high rates requiring multiple tests to detect all viruses present [1,7]. Sampling grapevines and testing is also time consuming and expensive. Since effective control and treatments for the grapevine virus have not been developed yet, recommendations are to remove infected vines before they act as a source of transmission in the vineyard. There is an urgent demand to develop an efficient method for the rapid and early detection of viruses. There has been good progress in using remote sensing technology to detect the spatial allocations and patterns of viticulturally meaningful variations such as water stress [8] and nutrient deficiency [9], yet further research is required to evaluate their effectiveness in detection of biotic stresses in vineyards.

An observation on the phenotypic changes induced by GLRaV-3 infection shows two distinct features: late season reddening of foliar tissues and interveinal reddening (primary veins remain green). The virus-infected leaves turn red primarily as a result of anthocyanin deposition [10] and transformation of the vein areas in the stressed leaves is also expected from the dilution effect of carbohydrate buildup

* Corresponding author.
E-mail address: leeko@bbbfly.com (L. Lee).

https://doi.org/10.1016/j.atech.2024.100464
Received 30 December 2023; Received in revised form 19 April 2024; Accepted 2 May 2024
Available online 5 May 2024

at the grape ripening period [11–13]. Pathogenic attacks initiate biochemical pathways, and the plant defense system responds to the threat of infection by pathogens in two different ways [14]. First, defenses are initiated by inducible mechanisms when pathogens are perceived as a threat and cause induction of defense pathways, even in the undamaged leaves of pest infested plants soon after attack [15]. The inducible defenses are still not completely understood, but changes and accumulations of papillae are observed as a physical barrier to prevent pathogens from accessing the inner cells of the plant [16]. The second mode of plant defense system, Hypersensitive Response (HR) is involved in defense mechanisms against pathogen infected cells limiting further pathogen multiplication and spread [17]. Stress activates the HR predominantly through reactive oxygen species (ROS) that oxidize polyunsaturated fatty acids with altering permeability and affect the structural integrity of cells [17].

A remote sensing application for agriculture uses electromagnetic waves to sense soil or plant matter. The majority of remote sensing applications involve measuring the reflected radiation instead of the transmitted or absorbed radiation [18]. Biological pigments absorb energy from photons of sunlight, which carry energy proportional to their radiation frequency [19–21]. Due to the role of pigment molecules in plant photosynthesis and stress responds, pigment content in leaves is a good indicator of plant health and photosynthetic activity [19]. The reductions in a plants' capacity for photosynthetic activity due to a stress could be demonstrated through changes in pigment quantities and ratios, which can significantly alter the plant's interaction with electromagnetic energy. Plants receive radiation on the wavelengths of 400-700 nm, which are absorbed by their pigment molecules and utilized for their individual energy potentials [22]. There are many other types of key pigment molecules in plants for remote sensing, such as carotenoids [23], flavonoids, and anthocyanins [24]. The Electromagnetic (EM) reflectance of vegetation in agriculture is measured in multiple wavelength bands, mostly the green, red, red edge and near-infrared bands (NIR) and the reflectance is computationally transformed to the variable indices [25]. Different factors have a profound impact on the reflectance levels in the visible, red edge, and NIR peaks. The visible region of the reflectance is influenced by pigment molecules, while changes in NIR spectrum are affected by variations in leaf arrangement and density [26]. The red edge peak is in the boundary between visible and NIR spectra and the peak is applied to calculate plant composition such as chlorophyll contents [27]. Previous research proved that chlorophyll concentration is negatively correlated to the EM reflectance at the red edge range and an increase in chlorophyll concentration shifts the inflection point of entering red edge region to higher wavelength [28–30]. The emission of fluorescence in red edge and NIR regions can also be an important electromagnetic signal for plant stress detection [31]. Chlorophyll fluorescence is an emitted light energy in photosynthetic tissues upon excitation with natural or artificial illumination in the red and red edge peak to disperse the excessive photosynthesis energy and to protect the chloroplast from oxidative damage [32]. Chlorophyll molecules in leaves can either facilitate photosynthesis, release heat or emit fluorescence, and these three processes are competitive, such that any increase in output in one affects the yield in the other two [32]. Photosystem II (PSII), a solar energy-harvesting component in higher plants, is regulated by external environmental factors [33]. Nonphotochemical quenching (NPQ) occurs when moderately excess light occurs without damaging PSII reaction centers. Unwanted energy is harmlessly released as heat while the photochemical quenching system is engaged [33].

A narrow spectral band sensor offers a lot of potential for remote sensing of plant stresses and especially for detecting virus infection [34], phylloxera infestation [35], and differences in nutrient status and uptake [36]. Portable spectrometers typically carry hundreds of bands and proved to have a potential application of remote sensing with many wavebands of spectral information [37]. Various crop health parameters are measured, including vegetation indexes and disease detection, by using portable sensors that can be hand-held or mobile for continuous and real-time observation [38]. This research aimed to develop a rapid and early detection method for GLRaV-3 infected vines using remote sensing data and we hypothesized that the presence of grapevine virus and its infected leaves have unique electromagnetic signatures at early stages of the virus development, which could be detected by a narrow-band, hyperspectral sensor. The representative vines of healthy and GLRaV-3 infection were selected by Real-Time reverse transcription quantitative polymerase chain reaction (RT-qPCR) test. The effects of biotic stress from GLRaV-3 infections on changes of electromagnetic (EM) reflectance spectrum of leaves were examined by hand-held hyperspectral spectrometer and multispectral sensor attached on a remotely piloted aircraft system (RPAS). To discover the early-stage spectral signatures of the virus infected leaves, the effect of visible symptoms of virus infection on the EM reflectance was also investigated by differentiating the EM spectra of virus asymptomatic leaves (early stage of virus infection) from these of healthy and virus symptomatic leaves.

Materials and Methods

Experimental Setup

Vine selection and GPS delineation were performed prior to the research data collection. An initial data collection phase, including RPAS flight and leaf sampling for the PCR test, was performed in September 2016 to determine whether VIs from RPAS maps could be used to determine potential virus infections. The second phase of data collection with a hyperspectral spectrometer involved investigating leaf reflectance in more detail in the following season (2017) due to the lack of correlation between the conventional VIs and infection in 2016 data. The GPS delineated vines for the research were not removed between the two phases.

Research vines selection and GPS-delineation

This project involved two GLRaV-3 infected Cabernet franc vineyard blocks located within the Niagara Peninsula of Ontario, Canada. The representative vines of healthy and the GLRaV3 infection were selected and geolocated for detecting the virus by Real-Time reverse transcription quantitative polymerase chain reaction (RT-qPCR) test and for measuring spectral reflectance by a hand-held spectrometer and remotely piloted aircraft system (RPAS). Invicta 115 GPS receiver (Raven Industries, Sioux Falls, SD) technology was applied to geolocate the research vines. The Invicta 115 receiver provides a 1 to 1.4m accuracy, which was improved further with a subsequent adjustment with the Port Weller, Ontario base location, resulting in a closing precision of 30 to 50 cm.

PCR test for presence of grapevine leafroll-associated virus (GLRaV)

In September 2016, three leaves were sampled from three different sections of vine canopy for Real-Time RT-qPCR test at the Molecular Biology lab at the University of Guelph (Guelph, Ontario). The leaves were powdered and placed in liquid nitrogen and frozen at -80°C. In this study, the RNA isolation method was used to isolate total RNA from samples, and Nanodrop spectrophotometers were used to measure RNA concentrations and quantities. A High-capacity cDNA Reverse Transcription Kit was used to prepare cDNA. Random hexamer sequences from the coat protein gene were used as a primer, the part of the genome that is most conserved in GenBank through sequence alignment using DNASTAR's MegAlign program. A two-primer test was conducted on all samples to ensure the reliability of the data (Supplemental Table1 and 2). The first set of primers of GLRaV was used for conventional reverse transcription polymerase chain reactions (RT-PCR), followed by testing the second pair of primers using a two-step SYBR Green real-time RT-

PCR assay, which the virus titer in leaves was quantitatively compared between plants. Actin was applied as a reference gene, a reliable marker for grapevines' response to a stress [39]. GLRaV-3 presence was calculated from the PCR results, where a higher score reflects less virus presence.

Electromagnetic (EM) reflectance data collection by remotely piloted aircraft system (RPAS)

The eBee Classic RPAS (Parrot group, Switzerland) was flown during veraison in 2016 with an altitude of 90 m and a maximum speed of 60 km/h. The Sequoia multispectral sensor (Parrot Group, Switzerland) was selected for collecting spectral data and it was equipped with an incident light sensor of 1.2 megapixels (1280 × 960 pixels)and a pixel size of 3.75 μm, which represented a spatial resolution of 8.47 cm on the ground at the 90 m altitude. Images were collected in the visible and near-infrared (NIR) regions of reflectance with four wide bands (green: 530-570 nm, red: 640-680 nm, red edge: 730-740 nm, and the near infrared: 770-810 nm). Additionally, the aircraft featured a GPS receiver, radiation monitor estimating inbound radiation, and an inertial system for maintaining the alignment and positioning of imaging. The RPAS also had an autopilot system that provided a visual range of 1000 m and a radio range of 5 km. The vehicle was powered by an electric motor with a battery life of 50 minutes. Air-Tech Solutions, Inverary, ON, provided a RPAS and its ground control station for real-time tracking and collection of images over each vineyard patch. The RPAS was equipped with a GPS receiver, sunshine sensor measuring incoming radiation, and an inertial station ensured verticality and orientation of images by correcting anomalies in flight attitude (i.e., yaw, pitch, and roll). Based on the data from the inertial station and radiation sensor, geometric and imaging adjustments were performed for geometry, reflectivity, image distortions, sun exposures, and vignetting effects in radiometric. A geometric correction using ground control points (GCPs) was performed to adjust the geometry of the image and adjust the bidirectional reflectance for ensuring the accuracy and consistency of data. Geometric distortions caused by changes in RPAS attitude and altitude were corrected using the information provided by the inertial station. Radiometric correction was performed to correct effects of vignetting. Data were also adjusted for the input of the sunshine sensor before the reflectance generation. Indices were calculated from the mosaics assembled from the images acquired on each phase of each flight by choosing overlapping pixels near nadir to minimize the problems of angle distortion and directional effects during the images acquisition.

Electromagnetic (EM) reflectance data collection by portable spectrometer

With a portable spectrometer model EPP2000C and SpectraWiz software (StellarNet Inc., Tampa, FL), the reflectance spectra of the leaves were obtained and analyzed with a 400-850 nm range and a resolution of 1 nm per pixel. In this experiment, a 5-watt halogen bulb illuminated the entire surface of a leaf placed on a dark plate, and a fiber optic cord designed to capture the reflected spectra at 45°angle to the leaf surface. An optical spectrum of the white and dark surface was referenced frequently at every 10th measurement using a white Teflon® square and black surface pad. The spectral measurement was performed in September 2017 after the virus presence data for three strains of GLRaV-1, 2, and 3 had been obtained from Real-Time RT-qPCR test. A total of 150 leaf samples comprising 75 leaf samples from each site (25 from healthy vines, 25 from asymptomatic vines, and 25 from symptomatic vines) were measured from the two different GLRaV3 infected sites and were pictured in the photos shown in Supplemental Fig. 1. The virus-positive Cabernet franc leaves demonstrated common signs of GLRaV-3 during scouting spectral measurements by the portable spectrometer in September 2017 [Supplemental Fig. 1 (a)]. Previous study indicated that a visual symptom of GLRaV infection was distinct at later season [1,3]. Therefore, the late growing season measurements were used to distinguish asymptomatic leaves from symptomatic leaves. On the leaf blades of infected grapevines, the interveinal spaces contained purple pigmentation and veins appeared to have a slight band of greenish tissue on both sides. However, some GLRaV-3 positive vines remained asymptomatic [Supplemental Fig. 1 (b)]. All grapevines that tested negative for GLRaV-3 had healthy leaves without any virus symptoms [Supplemental Fig. 1 (c)].

Data analyses

Mapping and data extraction

dGPS coordinate points (latitude, longitude) as well as values from all manually collected variables were imported into ArcMap 10.6 and inverse-distance-weighted (IDW) used sampled values to estimate values at unsampled locations. In a spatially discretized way, IDW uses a linearly weighted set of data points to calculate a point's value, where the weighted average of points sampled declines with rising gap from the unsampled location [40]. Two major parameters exist in determining the accuracy of the IDW interpolations: power and search radius. IDW relies mainly on the inverse of the distance between known and unknown locations, raised to a mathematical power, which controls the significance of known points on the interpolated values based on their distance from the output point. The search radius controls the input points used in the calculation of each output cell value. Several trials of different combinations of power and search radius were made to identify parameters for IDW that created the most accurate maps but at the same time maintained readable and interpretable maps during this study. For instance, the highest and lowest values of original data were compared to those data from IDW and it only created the projected pattern from local variation and did not interrupt any original dataset. A higher power puts more emphasis on the nearest points, and for this study the default value of 2 was used. A fixed search radius was used as follows: Standard Sector - Four Sectors with 45° offset; minimum neighbors: 10, maximum: 15.As a data classification method, Quantile breaks were used, which classified the data with the same number of elements in each class, and thereby avoided extraordinarily large or empty classes and facilitating the interpretation of the maps. In remote sensing applications with dense spatial data, diffusion interpolation with a smaller spatial channel enables efficient interpolation and a seamless contour plot using the same class and colour rules as IDW method. Interpolation spatial methods also enable the extraction of spectral values at the GPS coordinated research vines from surrounding sampled data. For all remote sensing indices creation, the flight data were imported and displayed in ArcMap 10.6 with World geodetic system 1984 and projected in the Universal Transverse Mercator zone 17N. Using the IDW interpolation technique and the extract values to point tool, the resultant data were interpolated and further exported to Microsoft Excel sheets in which each study vine was associated with its dGPS coordinate points as well as data from the RPAS flight. In Table 1, Multiple indices can be calculated based on the green, red edge, and NIR regions of multispectral imagery to characterize virus detection according to previous studies [41,42].

Table 1
Remote sensing indices to characterize vine health and virus infections.

Remote sensing Indices	Equation
NDRE (Red Edge Normalized Difference Vegetation Index)	(NIR − Red Edge)/ (NIR + Red Edge)
GNDVI (NDVI Green)	(NIR − Green)/ (NIR + Green)
GRVI (Green-Red Vegetation Index)	(Green − Red)/ (Green + Red)
MTCI (MERIS Terrestrial Chlorophyll Index)	(NIR − Red Edge)/ (Red Edge + Red)
RTVI core (Core Red Edge Triangular Vegetation Index)	100(NIR – Red Edge) − 10(NIR − Green)

Correlation-based analyses

Indices from the multi-spectral data of the RPAS flight in 2016 were extracted and examined to characterize vine health and GLRaV3 detection. To run correlation-based analyses, designated clean vines by Real-Time RT-qPCR were assigned a "0" and GLRaV3 infected vines were assigned a "1". Principal component analysis PCA and Pearson's correlations analysis were performed to compare GLRaV3 presence against the extracted remote sensing indices through XLSTAT v2021. The Shapiro-Wilk test was applied to each data to verify normality and any outliers were highlighted on boxplots after careful evaluation of the data variation. Prior to the next step to perform PCA, data were standardized. With PCA, a complex data set can be reduced to simple data that still contains most of the original data, and data correlated with one another can be transformed into principal components, starting with the first component describing most of the variance in the data. Each value in the first two factors was evaluated using the square cosine of the value to determine the level of relationship between the value and the axis, as part of the PCA analysis. Square cosine near zero of short vectors are indicators that the model does not adequately explain the relationship.

Portable spectrometer data analysis

The line graphs of mean electromagnetic (EM) reflectance for leaves from healthy and GLRaV3 infected grapevines were used to display the visual difference between the treatments. The two tailed t-tests and column charts of mean value were also conducted to confirm that different reflectance levels occurred through visible and NIR wavebands among symptomatic, asymptomatic, and healthy leaves.

Results

Detection of grapevine leafroll associated virus (GLRaV)-1,2,3 infection by Real Time qPCR

In this study, two Niagara Peninsula Cabernet franc vineyard sites were examined for the presence of GLRaV-1, -2, -3. In Table 2, no samples were infected by GLRaV-1 and only one vine was infected by GLRaV-2 across the sites, so all statistical analyses were confined to determining GLRaV-3 presence only. Near the time of the RPAS flight, a random sample was taken of upper, middle, and lower leaves of Cabernet franc vines in September 2016.

Relationships between remote sensing data from RPAS flight and GLRaV-3 infection

Multiple remote sensing indices can be calculated based on the green, red edge, and NIR regions of multispectral imagery to determine whether vines are infected with viruses. In Table 1, The indices were characterized virus detection according to previous studies [41,42]. Fig. 1, over 83 % of the data for GLRaV-3 detection in each site was explained by PCA models based on the first two factors. The GLRaV-3 infection positively correlated to NDRE in site 1 and to RTVIcore in site 2 but in both sites, vectors for GLRaV-3 infection were short, making visual comparisons challenging. According to Pearson's correlation analysis did not detect a correlation between the remote sensing indices and GLRaV-3 infection (Table 3).

Spectral measurements of healthy and GLRaV3 infected leaves by the hand-held spectrometer Wine chemical analysis. To determine if visible symptoms affected the remote sensing indices and wavelength bands, the electromagnetic spectrum of symptomatic and asymptomatic GLRaV-3-infected leaves were presented separately. EM reflectance differences between asymptomatic and healthy leaves were observed throughout the spectra (Figs. 2 and 3).

The different EM reflectance peaks were segregated based on the inflection point of each band from Figs. 2 and 3: the green (500-600 nm), the red (630-700 nm), the red edge (701-740 nm), and the NIR (741-849 nm). The EM reflectance differences between symptomatic and asymptomatic leaves were more prominent than the differences between symptomatic and healthy leaves in green and red regions. GLRaV-3 asymptomatic leaves also had substantially higher light reflectance levels than those of healthy and symptomatic leaves throughout the visible regions. The reflectance in GLRaV-3 symptomatic leaves had substantially lower light reflectance levels than these of healthy and symptomatic leaves at green and part of red regions. The symptomatic leaves had a reflectance hike at the red edge peak. This trend continued extending into the NIR region with a bigger increase (Figs. 2 and 3). The t-test results also confirmed that different reflectance levels occurred in these regions among symptomatic, asymptomatic, and healthy leaves (Figs. 4 and 5).

Red edge spectral shifts from these leaf samples were also investigated. Red edge inflection point (REIP), also known as red edge position (REP) is the maximum first derivative of red edge reflectance and was based on the formula [43]: REIP=MAX(nm) $\frac{R(n+1)-R(n)}{WAVELENGTH(n+1)-WAVELENGTH(n)}$ = MAX(nm) $\frac{R(n+1)-R(n)}{1}$ = Max R(x), Rn = reflectance value at wavelength n, R(n+1) = reflectance value at

Table 2
Real-Time qPCR results in the presence of GLRaV-2 and -3 for grapevine leaf samples collected from two study sites. "-"indicated negative result, "+" indicated cycle threshold (CT) value in the range of 36 to 38, "++" indicated CT value below 35.

Site	Row	Panel	GLRaV-1	GLRaV-2	GLRaV-3	Site	Row	Panel	GLRaV-1	GLRaV-2	GLRaV-3
1	3	9	–	–	–	2	4	12	–	–	–
	3	24	–	–	–		4	37	–	–	+
	3	39	–	–	–		7	37	–	–	–
	7	39	–	–	++		7	22	–	–	–
	7	24	–	–	+		7	7	–	–	++
	7	9	–	–	–		10	12	–	–	–
	11	9	–	–	++		10	37	–	–	+
	11	24	–	–	–		13	37	–	––	–
	11	39	–	–	+		13	22	–	–	+
	15	39	–	–	+		13	7	–	–	–
	15	24	–	–	–		16	12	–	–	–
	15	9	–	+	+		16	37	–	–	–
	19	9	–	–	–		19	37	–	–	–
	19	24	–	–	++		19	22	–	–	–
	19	39	–	–	+		19	7	–	–	–
							22	12	–	–	++
							22	37	–	–	–
							25	37	–	–	–
							25	22	–	–	++
							25	7	–	–	++

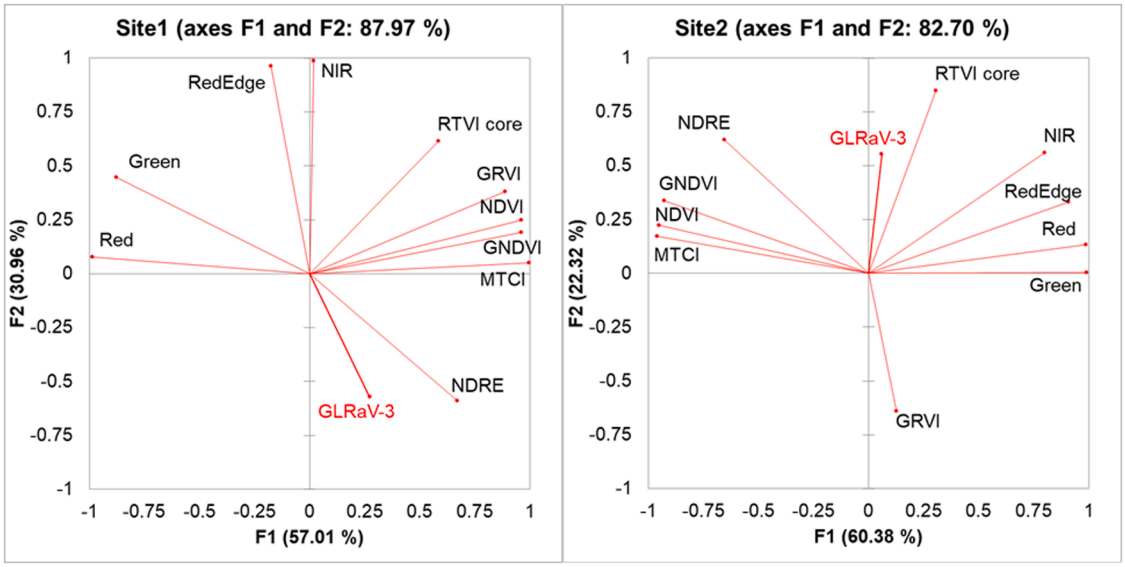

Fig. 1. PCA results for GLRaV-3 presence vs. remote sensing indices including green, red, red edge, NIR, NDVI, NDRE, GNDVI, GRVI, MTCI, and RTVI core. Abbreviations: NIR= Near infrared, NDVI= Normalized difference vegetation Index, NDRE= Red edge normalized vegetation index, GNDVI= NDVI green, GRVI= Green-red vegetation index, MTCI= MERIS terrestrial chlorophyll index, RTVI core= Core red edge triangular vegetation index.

Table 3
Pearson's correlation results between GLRaV-3 presence and remote sensing indices in the two virus infected vineyards. Abbreviations: NIR= Near infrared, NDVI= Normalized difference vegetation Index, NDRE= Red edge normalized vegetation index, GNDVI= NDVI green, GRVI= Green-red vegetation index, MTCI= MERIS terrestrial chlorophyll index, RTVI core= Core red edge triangular vegetation index.

	Correlation matrix		p-values	
Variables	Site1	Site2	Site1	Site2
Green	−0.449	0.016	0.093	0.948
Red	−0.295	0.076	0.286	0.750
Red Edge	−0.471	0.272	0.076	0.246
NIR	−0.443	0.323	0.098	0.164
NDVI	0.140	0.064	0.618	0.787
NDRE	0.393	0.075	0.147	0.755
MTCI	0.213	0.064	0.445	0.789
RTVI core	−0.173	0.258	0.538	0.272
GNDVI	0.190	0.138	0.498	0.561
GRVI	−0.014	−0.291	0.962	0.213

wavelength n+1, R(x)' = first derivative of reflectance change (slope of reflectance graph).

The REIP results are shown in Figs. 6 and 7, which indicate that both in site 1 and site 2, virus symptomatic leaves had the lowest REIP while asymptomatic and healthy leaves showed the REIP shifted to higher wavelength.

In the red and red edge regions, the relative reflectance changes (ΔRn) were determined for the different treatments to observe the rate of change based on reflectance values at each wavelength. The relative reflectance change (ΔRn) from one wavelength to another was calculated from the formula [44]:

$$\Delta Rn = \frac{R(n)'}{R(n)} = \ln(R(n))' = \frac{d\ln(R(n))}{dn} = \lim_{h-1} \frac{\ln(R(n+h)) - \ln(R(n))}{h} = \ln(R(n+1)) - \ln(R(n)).$$

The MaxΔRn results are shown in Figs. 8 and 9, which indicate a smooth and clear trend at the inflection point for all three treatments with the ranges of inflection point between 698 nm and 702nm. The relative data also indicated that the relative changes were lower in virus asymptomatic leaves than these in virus symptomatic and healthy leaves at the inflection point.

Discussion

Remote sensing indices from the multi-spectral data of the RPAS flight were extracted and examined to characterize vine health and virus detection. Although previous studies demonstrated the potential for grapevine virus detection using multispectral sensors on RPAS's [45-48], the results of correlation coefficient test in this study indicated that there were no significant correlations found among any of the RPAS remote-sensing indices and the occurrence of the GLRaV-3 (Table 3). The absence of any correlation between the virus infections and remote sensing indices could be caused by a number of factors. It is possible that the multi-spectral data acquisition occurred prior to the development of GLRaV-3 symptoms. The virus symptoms appear in the late ripening period as a result of source-sink dynamics that interfere with carbohydrates being transported from the leaves to the berry tissues, leading to accumulation of carbohydrates in the leaves [12]. Carbohydrate accumulation in mesophyll cells inhibits photosynthesis and promote the accumulation of flavanols and anthocyanins for mitigating photo-oxidative damage via upregulated expression of MYB type transcription factors [13,49]. Another possible explanation of the absence of correlation could be limitations of spatial and spectral resolution of the multi-spectral sensor measurement from RPAS flight. Multispectral sensors have spectrally broad bands with integration of tens of nanometers into one band leaving gaps between different bands and therefore, they are not able to reconstruct a detailed continual reflectance of plant canopy [50]. In this study, multi-spectral images were collected in the visible and near-infrared (NIR) regions of reflectance with four wide bands (green: 530-570 nm, red: 640-680 nm, red edge: 730-740 nm, and the near infrared: 770-810 nm). Based on the results of this study, a wavelength around 700 nm in the reflectance spectrum could be effective for identifying viruses, but the multi-spectral sensor did not include this wavelength. It proposed future supplement research to investigate 630-700nm of multi-spectral band using the RPAS flight.

In the following season (2017), leaf reflectance was investigated in greater detail with a hyperspectral spectrometer due to the lack of correlation between the virus infections and muti-spectral data in 2016. The results of hyperspectral spectrometer revealed some distinct outcomes that need further investigation. First, GLRaV-3 asymptomatic leaves had substantially higher light reflectance levels than these of healthy and symptomatic leaves throughout the visible (green and red), and red edge spectra. Plant leaf surfaces are at the front line to fight

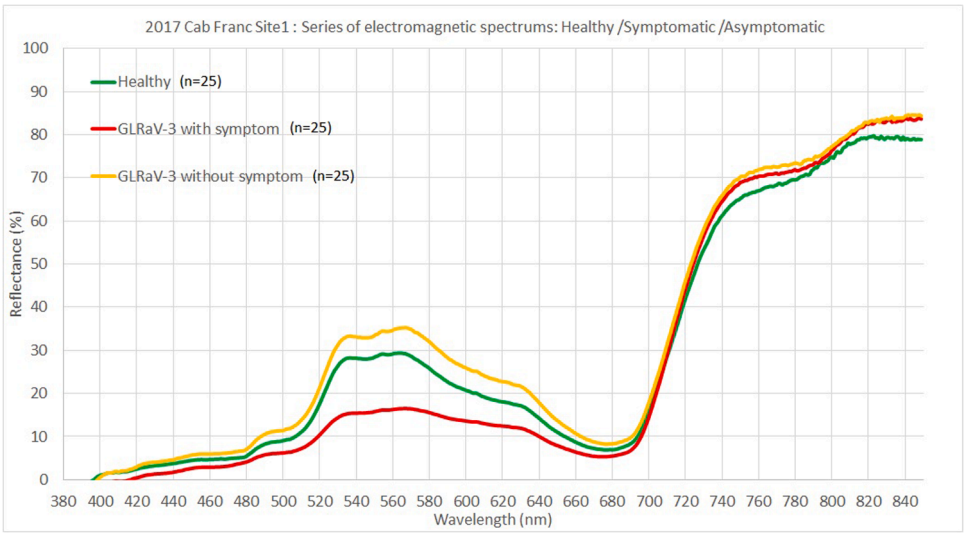

Fig. 2. The series of electromagnetic spectra from healthy and GLRaV-3 symptomatic and asymptomatic Cabernet franc leaves measured by hand-held spectrometer at site 1. The reflectance(%) was average of each treatment in steps of 1 nm wavelength.

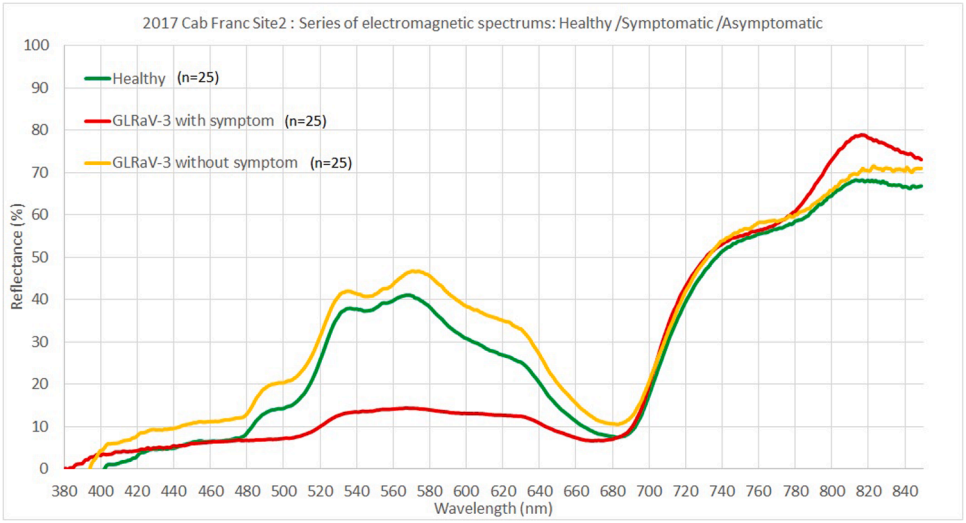

Fig. 3. The series of electromagnetic spectra from healthy and GLRaV-3 symptomatic and asymptomatic Cabernet franc leaves measured by hand-held spectrometer at site 2. The reflectance(%) was average of each treatment in steps of 1 nm wavelength.

against any biotic stresses with altering its cell wall structure and providing a protection against pathogens [51]. The first defense system of plants is induced by infection with GLRaV-3, resulting in hardening of leaf surfaces to stop invading pathogens. Hence, the observation of higher light reflectance in asymptomatic leaves with GLRaV-3 infection in this study may be associated with the hardening of the leaf surface walls at an early stage of infection, preventing light penetration and absorption. Secondly, the EM reflectance in GLRaV-3 symptomatic leaves had substantially lower light reflectance levels than these of healthy and asymptomatic leaves in the visible (green and red) regions where the leaf reflectance is dominated by ability of absorbing light energy by leaf pigments [52]. Since the symptomatic leaves indicated the reduction in chlorophyll concentration and its negative impacts on absorbing red light for photosynthesis, the higher reflectance level was expected in the symptomatic leaves in the red trough [52]. The abnormality between the reflectance of red peak and the virus symptomatic leaves in this study could be explained by presence of the second mode of plant defense system, known as hypersensitive response (HR), in the GLRaV-3 symptomatic leaves. The GLRaV-3 symptomatic leaves were at the later stage of the virus infection and triggered HR dominated plant defense response against the virus infection. Therefore, the HR may induce a structural change at the leaf surface, which diminishes the specular reflectance as each ray of the beam encounters different geometric angles in the red region. Previous studies also confirmed that increases in leaf transmittance and decreases in leaf absorbance levels in the EM spectrum were observed in the stressed plants [53,54]. Another notable spectral observation of the GLRaV-3 infected leaves was the symptomatic leaves had a reflectance hike at the red edge peak. This trend continued extending into the NIR region with a bigger increase. An increasing light emission rate of the chlorophyll fluorescence in the virus symptomatic leaves may cause the reflectance increase in red edge and NIR regions. Chlorophyll fluorescence is inversely related to photosynthetic rates and the symptomatic leaves with severe stress conditions may trigger activation of HR and induce a collapse of chlorophyll activity and decrease in photosynthesis rates [55,56]. Lastly, The degradation of chlorophyll in the virus symptomatic leaves was observed by comparing the red edge inflection point (REIP) index extracted from the EM reflectance of three virus infection treatments [57]. The REIP is

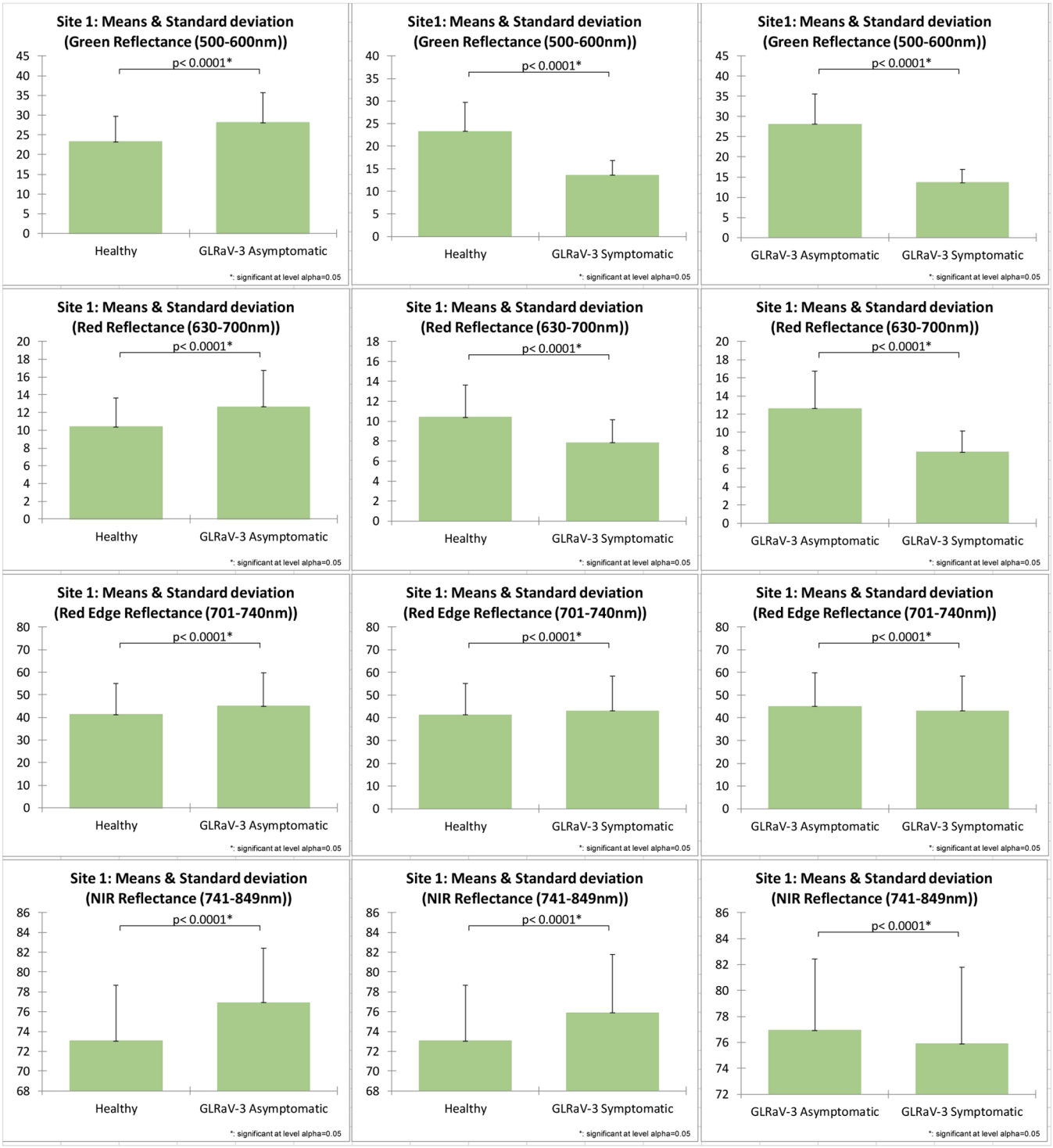

Fig. 4. Comparison of mean reflectance (%) of EM spectrums of green, red, red edge, and NIR peaks from healthy (n=25), asymptomatic (n=25) and symptomatic (n=25) GLRaV-3 infected Cabernet Franc leaves measured by hand-held spectrometer at site 1 using a t-test with two samples: * significant p-values (95 % confidence).

based on calculation of absolute reflectance changes to get the inflection point at the red edge spectrum. The virus symptomatic leaves had the lower REIP value than these of asymptomatic and healthy leaves in both sites indicating the lowest chlorophyll concentration in the virus symptomatic leaves and the higher chlorophyll concentration in the healthy and asymptomatic leaves (Figs. 6 and 7) [57]. Effects of relative reflectance changes (ΔRn) at the inflection point were also investigated. Both REIP and ΔRn measured the changes in reflectance at red edge peak; however, the nature of the data was different from each other. The REIP calculated by an absolute difference between the reflectance per each wavelength unit while ΔRn calculated by a relative rate change from the original reflectance. Mathematically, the former is the slope of the reflectance graph, and the latter is logarithmic reflectance difference between the wavelengths. Since logarithmic conversion transfers an exponential scale into a linear scale, the relative values could be a useful concept to compare numerical variables with quantities growing

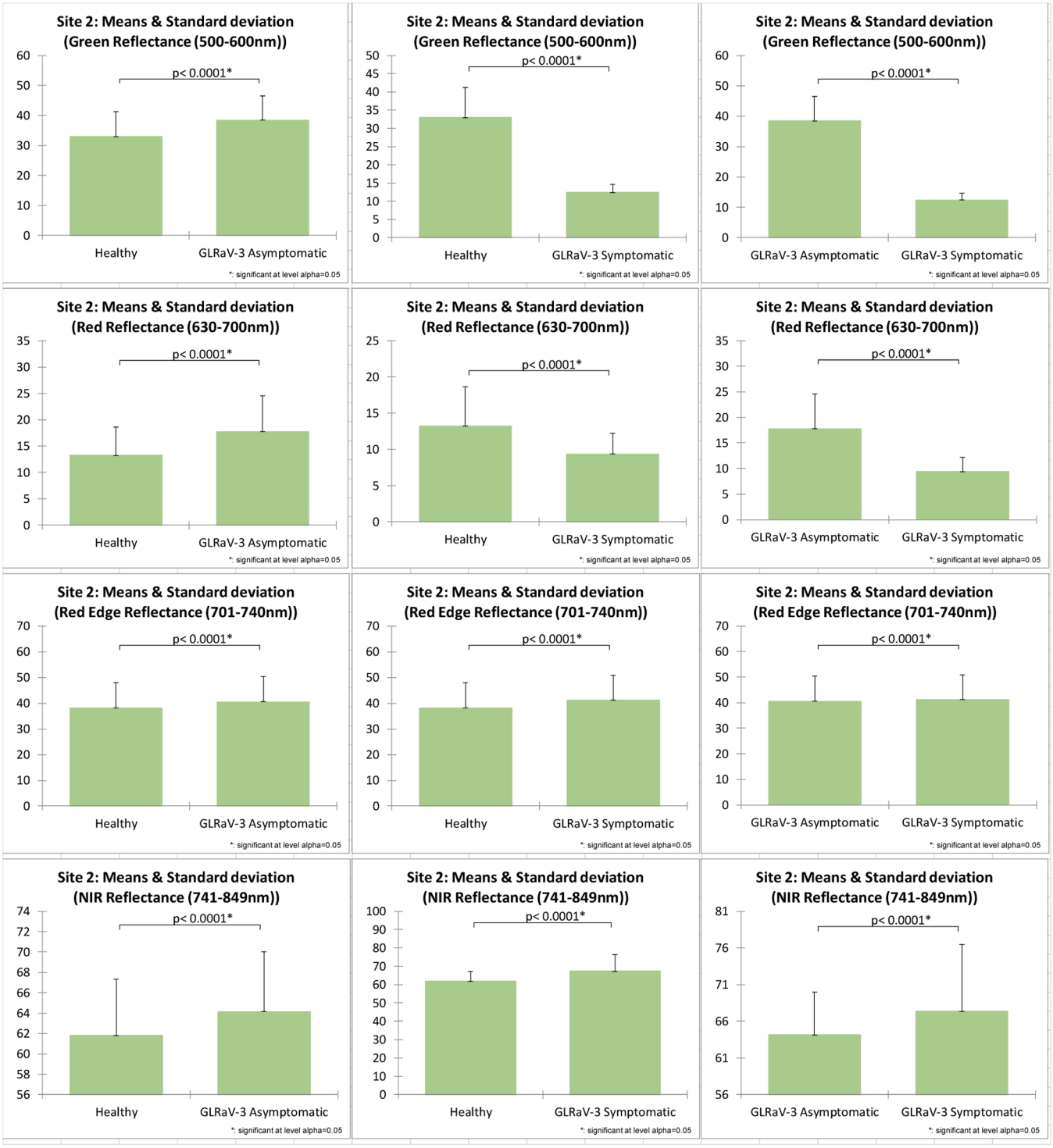

Fig. 5. Comparison of mean reflectance (%) of EM spectrums of green, red, red edge, and NIR peaks from healthy (n=25), asymptomatic (n=25) and symptomatic (n=25) GLRaV-3 infected Cabernet Franc leaves measured by hand-held spectrometer at site 2 using a t-test with two samples: * significant p-values (95 % confidence).

exponentially in the red edge peak [58]. The concept of relative difference also allows understanding of the comparative ratio of two numbers that gives us a direct insight into the true scale of difference between the treatments [58]. Interestingly, the relative rate changes of reflectance at red edge region were the highest (inflection point) around a certain wavelength (700 nm) throughout the treatments and sites and one could assume that a significant spectral incidence occurred at the inflection point in terms of the relative changes for different stages of virus infections. Results also indicated that the relative reflectance difference among the wavelengths was significantly lower in virus asymptomatic leaves and higher in virus symptomatic leaves around 700 nm (Figs. 8 and 9). The significant difference in rate increment of reflectance changes between the asymptomatic and symptomatic leaves around 700 nm could be induced by the chlorophyll fluorescence effect. The increment of reflectance change around 700 nm in the virus symptomatic leaves would lead to the assumption that a severe stress condition with

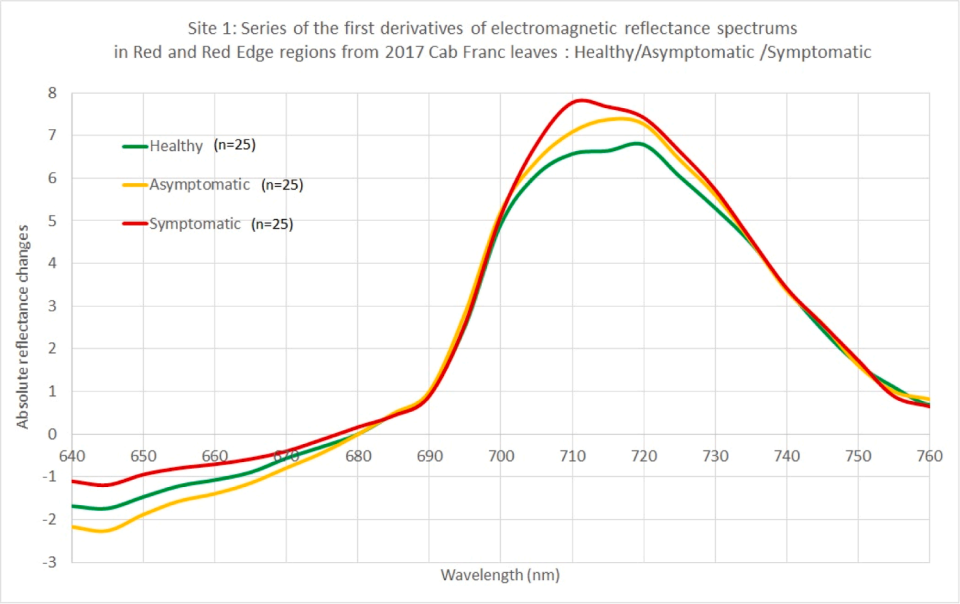

Fig. 6. The series of the first derivative values of electromagnetic reflectance spectra in red and red edge regions from healthy and GLRaV-3 symptomatic and asymptomatic Cabernet Franc leaves measured by hand-held spectrometer at site 1. The absolute reflectance change was average of each treatment in steps of 5 nm wavelength.

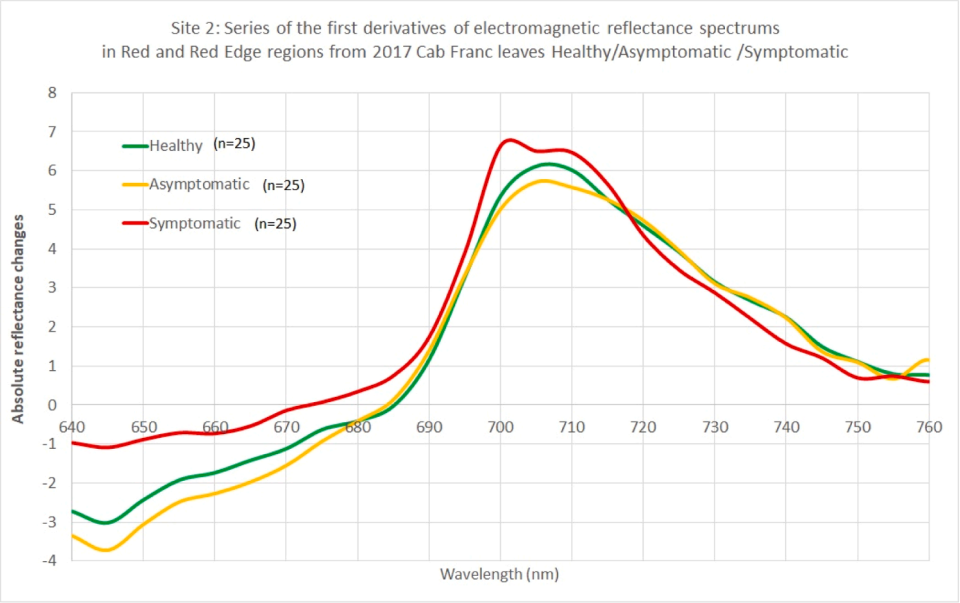

Fig. 7. The series of the first derivative values of electromagnetic reflectance spectra in red and red edge regions from healthy and GLRaV-3 symptomatic and asymptomatic Cabernet franc leaves measured by hand-held spectrometer at site 2. The absolute reflectance change was average of each treatment in steps of 5 nm wavelength.

activation of HR might also induce a collapse of the photosystem II activity, and the emission rate of chlorophyll fluorescence would increase with decreasing the NPQ activity and subsequent spike of the relative increment rate of EM reflectance observed around the certain peak (700 nm) in red edge range [55,56].

Conclusions and recommendations

Even though there were some experimental challenges such as visual assessment of virus symptoms, limited sample size, and time gaps between measurements, this study suggested that the response of individual foliar electromagnetic (EM) reflectance may differ due to an absence or presence of visible symptoms of infected leaves. The relative rate of reflectance changes around 700 nm could be an indicator for a dynamic light harvesting mechanism between energy utilization and dissipation in different stages of virus infection progress. While researchers demonstrated the feasibility of using multispectral sensors on RPAS to detect grapevine virus, none of the conventional spectral indices investigated in this study were consistent or robust enough to predict GLRaV-3 infection from the RPAS multi-spectral data. This study suggested selecting multispectral sensors with a wavelength near 700nm in the region of red or red edge for the remote sensing of early plant disease detection. The hyperspectral spectrometer data showed consistent and significant differences among the spectra of healthy,

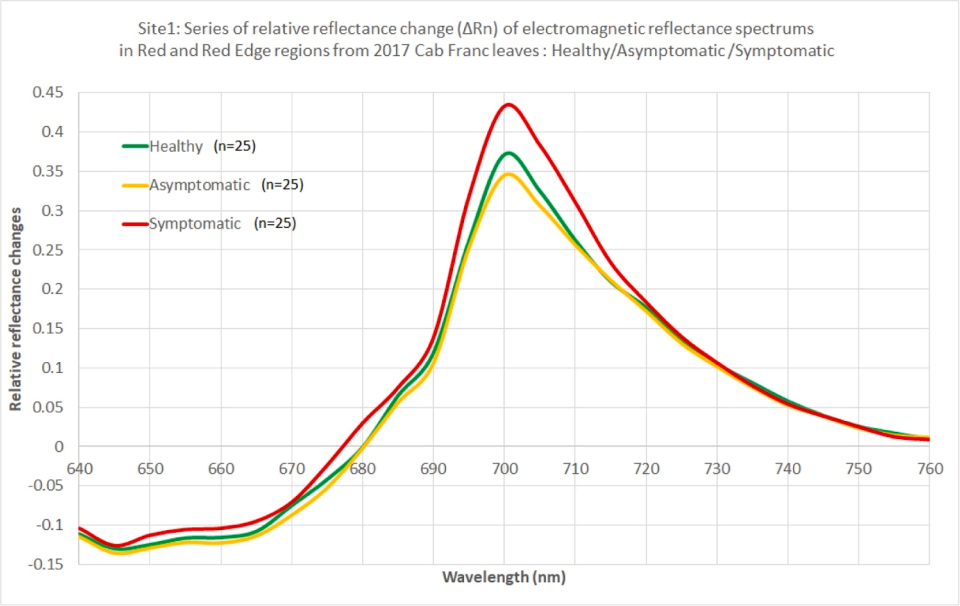

Fig. 8. The series of relative reflectance change (ΔRn) of EMS in red and red edge regions from healthy, GLRaV-3 symptomatic and asymptomatic Cabernet franc leaves measured by hand-held spectrometer at site 1. The relative reflectance change was average of each treatment in steps of 5 nm wavelength.

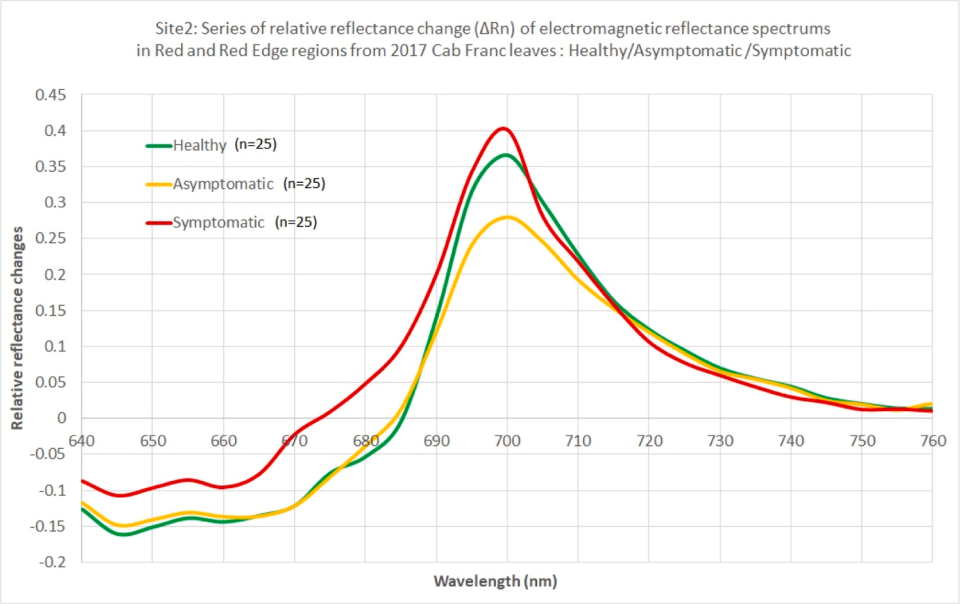

Fig. 9. The series of relative reflectance change (ΔRn) of EMS in red and red edge regions from healthy, GLRaV-3 symptomatic, and asymptomatic Cabernet franc leaves measured by hand-held spectrometer at site 2. The relative reflectance change was average of each treatment in steps of 5 nm wavelength.

asymptomatic, and symptomatic leaves. This finding leads to a recommendation for further study in a much more comprehensive investigation since there appears to be potential for development of a narrowband hyperspectral index for grapevine virus detection. For instance, a combination of hyperspectral sensor and chlorophyll fluorescence sensors may detect changes in leaf reflectance and emission from GLRaV-3 infection. This may warrant combination of suspect wavebands into ratios or indices. Concurrent virus titer and reflectance measurements along with much larger sample sizes and a more controlled environment would also be required.

Ethics Statement

Not applicable: This manuscript does not include human or animal research.

CRediT authorship contribution statement

Leeko Lee: Writing – review & editing; All data collection, analysis and interpretation of results. Andrew Reynolds: Study conception and design. Yibin Lan: Spectrometer data analysis. Baozhong Meng: PCR data acquisition and analysis. All authors reviewed the results and approved the final version of the manuscript.

Declaration of competing interest

The authors declare that they have no known competing financial interests or personal relationships that could have appeared to influence

the work reported in this paper.

Data availability

Data will be made available on request.

Acknowledgments/Author disclosures

We acknowledge cooperation and fruit donation from our collaborating vineyards in Niagara wine regions. We also acknowledge OMAFRA's New Directions Program for providing funds for the project.

Supplementary materials

Supplementary material associated with this article can be found, in the online version, at doi:10.1016/j.atech.2024.100464.

References

[1] H.J. Maree, R.P. Almeida, R. Bester, K.M. Chooi, D. Cohen, V.V. Dolja, M.F. Fuchs, D.A. Golino, A.E. Jooste, G.P. Martelli, Grapevine leafroll-associated virus 3, Front. microbiol. 4 (2013) 82.
[2] M.F. BaSSO, T.V. FAJARDO, P. SalDaRellI, Grapevine virus diseases: economic impact and current advances in viral prospection and management, Revista Brasileira de Fruticultura (2017) 39.
[3] R.A. Naidu, H.J. Maree, J.T. Burger, Grapevine leafroll disease and associated viruses: a unique pathosystem, Annu Rev. Phytopathol. 53 (2015) 613–634.
[4] O.J. Alabi, L.F. Casassa, L.R. Gutha, R.C. Larsen, T. Henick-Kling, J.F. Harbertson, R.A. Naidu, Impacts of grapevine leafroll disease on fruit yield and grape and wine chemistry in a wine grape (Vitis vinifera L.) cultivar, PLoS. One (2016) 11.
[5] S.S. Atallah, M.I. Gómez, M.F. Fuchs, T.E. Martinson, Economic impact of grapevine leafroll disease on Vitis vinifera cv. Cabernet franc in Finger Lakes vineyards of New York, Am. J. Enol. Vitic. 63 (2012) 73–79.
[6] F. Osman, C. Leutenegger, D. Golino, A. Rowhani, Comparison of low-density arrays, RT-PCR and real-time TaqMan® RT-PCR in detection of grapevine viruses, J. Virol. Methods 149 (2008) 292–299.
[7] H. Xiao, M. Shabanian, C. Moore, C. Li, B. Meng, Survey for major viruses in commercial Vitis vinifera wine grapes in Ontario, Virol. J. 15 (2018) 127.
[8] Z. Kandylakis, A. Falagas, C. Karakizi, K. Karantzalos, Water stress estimation in vineyards from aerial SWIR and multispectral UAV data, Remote Sens. (Basel) 12 (2020) 2499.
[9] S. Debnath, M. Paul, D.M. Rahaman, T. Debnath, L. Zheng, T. Baby, L. M. Schmidtke, S.Y. Rogiers, Identifying individual nutrient deficiencies of grapevine leaves using hyperspectral imaging, Remote Sens. (Basel) 13 (2021) 3317.
[10] L.R. Gutha, L.F. Casassa, J.F. Harbertson, R.A. Naidu, Modulation of flavonoid biosynthetic pathway genes and anthocyanins due to virus infection in grapevine (Vitis viniferaL.) leaves, BMC. Plant Biol. 10 (2010) 187.
[11] R. Turgeon, S.J.A.R.O.P.B Wolf, Phloem transport: cellular pathways and molecular trafficking, Annu. Rev. Plant Biol. 60 (2009) 207–221.
[12] D.K. Lee, S. Ahn, H.Y. Cho, H.Y. Yun, J.H. Park, J. Lim, J. Lee, S.W.J.S.R. Kwon, Metabolic response induced by parasitic plant-fungus interactions hinder amino sugar and nucleotide sugar metabolism in the host, Sci. Rep. volume 6 (2016) 1–11.
[13] H. Wan, J. Zhang, T. Song, J. Tian, Y.J.F.i.p.s Yao, Promotion of flavonoid biosynthesis in leaves and calli of ornamental crabapple (Malus sp.) by high carbon to nitrogen ratios, Front Plant Sci. 6 (2015) 673.
[14] J.D. Jones, J.L.J.N Dangl, Plant Immune System, Nature 444 (2006) 323–329.
[15] A. Steppuhn, I.T. Baldwin, Induced defenses and the cost-benefit paradigm. Induced plant resistance to herbivory, Springer, 2008, pp. 61–83.
[16] Nicaise, V.; Roux, M.; Zipfel, C.J.P.P. Recent advances in PAMP-triggered immunity against bacteria: pattern recognition receptors watch over and raise the alarm. 2009, 150, 1638-1647.
[17] P. Balint-Kurti, The plant hypersensitive response: concepts, control and consequences, Mol. Plant Pathol. 20 (2019) 1163–1178.
[18] C.F. Jordan, Derivation of leaf-area index from quality of light on the forest floor, Ecology 50 (1969) 663–666.
[19] J.P. Palta, Leaf chlorophyll content, Remote Sens. Rev. 5 (1990) 207–213.
[20] M.N. Merzlyak, A.A. Gitelson, O.B. Chivkunova, V.Y. Rakitin, Non-destructive optical detection of pigment changes during leaf senescence and fruit ripening, Physiol. Plant 106 (1999) 135–141.
[21] S. Pimputkar, J.S. Speck, S.P. DenBaars, S. Nakamura, Prospects for LED lighting, Nat. Photonics. 3 (2009) 180–182.
[22] S. Römer, P.D. Fraser, Recent advances in carotenoid biosynthesis, regulation and manipulation, Planta 221 (2005) 305–308.
[23] H.A. Frank, R.J. Cogdell, Carotenoids in photosynthesis, Photochem. Photobiol. 63 (1996) 257–264.
[24] L. Chalker-Scott, Environmental significance of anthocyanins in plant stress responses, Photochem. Photobiol. 70 (1999) 1–9.
[25] J. Arnó Satorra, J.A. Martínez Casasnovas, M. Ribes Dasi, J.R. Rosell Polo, Precision viticulture. Research topics, challenges and opportunities in site-specific vineyard management, Spanish J. Agricult. Res. 7 (2009) 779–790.
[26] Curran, P.J.J.R.S.O.E. Remote Sensing Of Foliar Chemistry. 1989, 30, 271-278.
[27] P.J. Curran, J.L. Dungan, H.L.J.T.p. Gholz, Exploring the relationship between reflectance red edge and chlorophyll content in slash pine, Tree Physiol. 7 (1990) 33–48.
[28] S. Ustin, S. Martens, B. Curtiss, V. Vanderbilt, Use of high spectral resolution sensors to detect air pollution injury in conifer forests. Remote Sensing Applications of Acid Deposition, EPA, 1988, pp. 72–85.
[29] D. Horler, M. DOCKRAY, J.J.I.J.O.R.S. Barber, The red edge of plant leaf reflectance, Int. J. Remote Sens. 4 (1983) 273–288.
[30] A.A. Gitelson, M.N. Merzlyak, H.K.J.J.O.P.P. Lichtenthaler, Detection of red edge position and chlorophyll content by reflectance measurements near 700nm, J. Plant Physiol. 148 (1996) 501–508.
[31] Kancheva, R.; Borisova, D.; Iliev, I. Chlorophyll fluorescence as a plant stress indicator. Recent Developments in Remote Sensing From Space 2008, 5, 301-306.
[32] A.M. Gilmore, How higher plants respond to excess light: Energy dissipation in photosystem II. Concepts in Photobiology, Springer, 1999, pp. 513–548.
[33] P. Horton, A. Ruban, R.J.A.R.O.P.B Walters, Regulation of light harvesting in green plants, Annu. Rev. Plant Physiol. Plant Mol Biol. 47 (1996) 655–684.
[34] S.L. MacDonald, M. Staid, M. Staid, M.L. Cooper, Remote hyperspectral imaging of grapevine leafroll-associated virus 3 in cabernet sauvignon vineyards, Comput. Electron. Agric. 130 (2016) 109–117.
[35] F. Vanegas, D. Bratanov, K. Powell, J. Weiss, F. Gonzalez, A Novel methodology for improving plant pest surveillance in vineyards and crops using UAV-based hyperspectral and spatial data, Sensors. (Basel) (2018) 18, https://doi.org/10.3390/s18010260.
[36] B. Gil-Pérez, P. Zarco-Tejada, A. Correa-Guimaraes, E. Relea-Gangas, L. Navas-Gracia, S. Hernández-Navarro, J. Sanz-Requena, A. Berjon, J. Martín-Gil, Remote sensing detection of nutrient uptake in vineyards using narrow-band hyperspectral imagery, Vitis 49 (2010) 167–173.
[37] S. Ryan, M. Lewis, Mapping soils using high resolution airborne imagery, Barossa Valley, SA, in: Proceedings of the Proceedings of the Inaugural Australian Geospatial Information and Agriculture Conference Incorporating Precision Agriculture in Australasia 5th Annual Symposium, 2001, pp. 17–19.
[38] Z. Li, J. Taylor, L. Frewer, C. Zhao, G. Yang, Z. Liu, R. Gaulton, D. Wicks, H. Mortimer, X. Cheng, A comparative review of the state and advancement of Site-Specific Crop Management in the UK and China, Front. Agricult. Sci. Eng. 6 (2019), https://doi.org/10.15302/j-fase-2018240.
[39] J.L. Coito, M. Rocheta, L. Carvalho, S. Amâncio, Microarray-based uncovering reference genes for quantitative real time PCR in grapevine under abiotic stress, BMC. Res. Notes. 5 (2012) 220.
[40] J. Li, A.D. Heap, A review of comparative studies of spatial interpolation methods in environmental sciences: Performance and impact factors, Ecol. Inform. 6 (2011) 228–241.
[41] F.-M. Wang, J.F. Huang, Y.L. Tang, X.Z.J.R.S. Wang, New vegetation index and its application in estimating leaf area index of rice, Rice Sci. 14 (2007) 195–203.
[42] D. Wu, L. Feng, C. Zhang, Y.J.T.O.T.A He, Early detection of Botrytis cinerea on eggplant leaves based on visible and near-infrared spectroscopy, Trans. ASABE 51 (2008) 1133–1139.
[43] A. Gholizadeh, J. Mišurec, V. Kopačková, C. Mielke, C.J.F Rogass, Assessment of red-edge position extraction techniques: A case study for norway spruce forests using hymap and simulated sentinel-2 data, Forests 7 (2016) 226.
[44] M. Lendar, A. Aissat, M. Cazaunau, V. Daële, A.J.C.P.L Mellouki, Absolute and relative rate constants for the reactions of OH and Cl with pentanols, Chem. Phys. Lett. 582 (2013) 38–43.
[45] S.F. Di Gennaro, E. Battiston, S. Di Marco, O. Facini, A. Matese, M. Nocentini, A. Palliotti, L. Mugnai, Unmanned aerial vehicle (UAV)-based remote sensing to monitor grapevine leaf stripe disease within a vineyard affected by esca complex, Phytopathol. Mediterr. 55 (2016) 262–275.
[46] J. Albetis, S. Duthoit, F. Guttler, A. Jacquin, M. Goulard, H. Poilvé, J.-B. Féret, G. Dedieu, Detection of flavescence dorée grapevine disease using unmanned aerial vehicle (UAV) multispectral imagery, Remote Sens. (Basel) 9 (2017) 308.
[47] M. Kerkech, A. Hafiane, R. Canals, Vine disease detection in UAV multispectral images using optimized image registration and deep learning segmentation approach, Comput. Electron. Agric. 174 (2020) 105446.
[48] H. Al-Saddik, J.-C. Simon, O. Brousse, F. Cointault, Multispectral band selection for imaging sensor design for vineyard disease detection: case of Flavescence Dorée, Adv. Animal Biosci. 8 (2017) 150–155.
[49] D.C. Close, C.L.J.T.B.R Beadle, The ecophysiology of foliar anthocyanin, Bot. Rev. 69 (2003) 149–161.
[50] A. Hall, D. Lamb, B. Holzapfel, J. Louis, Optical remote sensing applications in viticulture-a review, Aust. J. Grape Wine Res. 8 (2002) 36–47.
[51] C. Müller, M.J.J.O.C.E Riederer, Plant surface properties in chemical ecology, J. Chem. Ecol. 31 (2005) 2621–2651.
[52] S.L. Ustin, S. Jacquemoud, How the optical properties of leaves modify the absorption and scattering of energy and enhance leaf functionality, Remote Sens. Plant biodiversity (2020) 349–384.
[53] J.S. Schepers, T. Blackmer, W. Wilhelm, M. Resende, Transmittance and reflectance measurements of cornleaves from plants with different nitrogen and water supply, J. Plant Physiol. 148 (1996) 523–529.
[54] A.K. Knapp, G.A. Carter, Variability in leaf optical properties among 26 species from a broad range of habitats, Am. J. Bot. 85 (1998) 940–946.

[55] E.H. Murchie, T.J.J.O.E.B Lawson, Chlorophyll fluorescence analysis: a guide to good practice and understanding some new applications, J. Exp. Bot. 64 (2013) 3983–3998.
[56] P. Horton, M.P. Johnson, M.L. Perez-Bueno, A.Z. Kiss, A.V.J.T.F.j Ruban, Photosynthetic acclimation: Does the dynamic structure and macro-organisation of photosystem II in higher plant grana membranes regulate light harvesting states, FEBS J. 275 (2008) 1069–1079.
[57] O. Mutanga, A.K. Skidmore, Red edge shift and biochemical content in grass canopies, ISPRS J. Photogrammetry Remote Sens. 62 (2007) 34–42.
[58] S.E. Kastberg, Understanding Mathematical Concepts: the Case of the Logarithmic Function, University of Georgia, 2002.